Journal of Materials Chemistry A

Accepted Manuscript

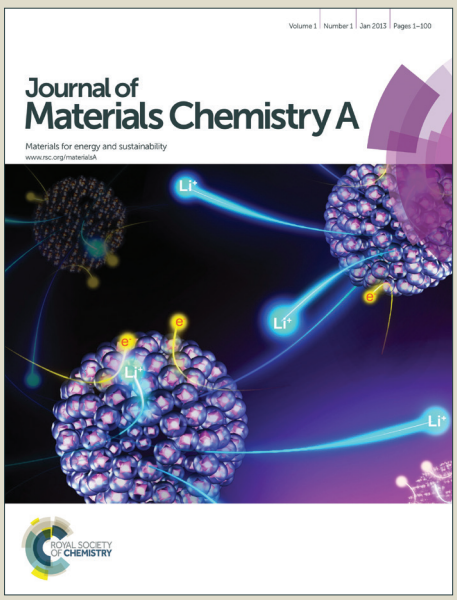

ROYAL SOCIETY OF CHEMISTRY

www.rsc.org/materialsA

Journal Name

RSCPublishing

ARTICLE

One-pot synthesis of carbon coated Fe_3O_4 nanosheets with superior lithium storage capability

Cite this: DOI: 10.1039/x0xx00000x

Guoxin Gao, Shiyao Lu, Bitao Dong, Zhicheng Zhang, Yuansuo Zheng, Shujiang Ding*

Received 00th January 2012,
Accepted 00th January 2012

DOI: 10.1039/x0xx00000x

www.rsc.org/

Hybrid nanosheet structures based on carbon coated metal oxides still attract promising interest as high-performance electrode materials for next-generation lithium-ion batteries (LIBs). In this study, we develop a simple one-pot solution method to synthesize the large-scale flat Fe_3O_4 nanosheet hybrid structures coated by amorphous carbon overlayer (denoted as Fe_3O_4@C NSs) followed by a thermal annealing treatment. It is found that the refluxing temperature plays an important role to adjust the morphology of Fe_3O_4@C hybrid. Upon increasing the temperature from 140 ^oC to 200 ^oC will lead to the flower-like hybrid structures constructed by Fe_3O_4 nanoflakes gradually growing, rupturing, and finally evolving into flat and completely separate nanoflakes with large size at 200 ^oC. When evaluated as an anode material for LIBs, the hybrid Fe_3O_4@C NSs demonstrate high reversible capacity of 1232 mAh g^{-1} over 120 cycles at the current density of 200 mA g^{-1}, and remarkable rate capability.

Keywords: Nanosheet; Fe_3O_4; Lithium-ion battery; Capacity.

1. Introduction

Rechargeable lithium-ion batteries (LIBs) have been widely used in portable electronic devices in the last two decades and recently have attracted extensive attention as power sources for electric vehicles (EVs) or hybrid electric vehicles (HEVs).[1-3] To cater to the requirements of practical applications in EVs or HEVs, exploring new electrode materials with high capacity and excellent stability is crucial for high performance LIBs because the total performance of LIBs highly depends on the electrochemical properties of these electrode materials.[4, 5] To date, transition metal oxides (TMOs), such as Co_3O_4,[6] TiO_2,[7] FeO_x,[8, 9] MnO_x[10, 11] have gained enormous research interest as promising anode materials for LIBs due to their higher specific capacities than that of the commercial graphite. Among TMOs, magnetite (Fe_3O_4) has received particular attention because of its low cost, eco-friendliness, natural abundance, and high theoretical capacity (928 mAh g^{-1}).[12] Unfortunately, Fe_3O_4-based anode usually suffers from poor rate capability and rapid capacity fading upon cycling caused by kinetic limitations, agglomeration and volume expansion during the conversion reaction process, thus hindering its practical application in next-generation LIBs.[13]

In order to overcome the above intractable problems, two representative strategies have been widely practised.[12-14] One popular strategy is to synthesize nanosized Fe_3O_4-based electrode materials with various morphologies, including nanoparticles,[15] nanosheets,[16] nanowires,[17, 18] nanotubes,[19, 20] and hollow nano-structures.[21, 22] Particularly, there is an increasing interest in fabricating two-dimensional (2D) porous nanosheet structures as electrodes for LIBs.[16, 23-25] More importantly, it has been found that the 2D porous nanosheet structure is beneficial for achieving high specific capacity and stable rate performance because the large specific surface area and the abundant active sites on the nanosheets both facilitate electron and lithium ion transport.[26] Another efficient strategy is combining Fe_3O_4 with carbonaceous materials, because these carbonaceous materials not only increase the electrical conductivity of the active materials but also suppress the particle aggregation, as well as the buffering effect for large volume changes.[12, 27-30] For example, carbon nanocoating has become a promising method to improve the electrochemical performance of the electrode materials.[31-34] However, carbon nanocoating reported recently usually requires an additional step to deposit a layer of amorphous carbon on the surface of the pre-synthesized electroactive material, which complicates the synthesis scheme.[35] Therefore, it is more desirable to develop a simple one-pot strategy to introduce the amorphous carbon overlayer in the electroactive Fe_3O_4 nanosheet/nanoflake composites.[36]

Herein, we develop a simple one-pot solution method to prepare the large-scale flat Fe_3O_4 nanosheets coated by amorphous carbon overlayer (denoted as Fe_3O_4@C NSs) followed by a thermal annealing treatment using ethylene glycol as the solvent and carbon source. The dispersed nanosheet morphology formed highly depends on the refluxing temperature. When evaluated as an anode material for LIBs, the as-prepared Fe_3O_4@C NSs hybrid composites exhibit remarkable lithium storage properties with high specific capacity, good cycling stability and excellent rate capability, all of which make it a promising anode material for high-performance LIBs.

2. Experimental part

***Materials synthesis*:** All of the chemicals were supplied by Sigma-Aldrich with analytical grade and used as received. In a typical synthesis of dispersed Fe_3O_4@C NSs hybrid composites, 0.54 g of $FeCl_3 \cdot 6H_2O$, 1.20 g of urea and 2 g of poly(vinyl pyrrolidone) (PVP, molecular weight 40 000) were added into 90 mL of ethylene glycol (EG) under magnetic stirring for about 30 min to form a cloudy solution. Then the resulting mixture was transferred into a round-bottom flask (250 mL) and refluxed in an oil bath at 200 ^oC for 1 h under violently magnetic stirring. After cooling down to room temperature naturally, the product was harvested by centrifugation and washed with absolute ethanol for several times. Finally, the obtained precursors were dried at 80 ^oC in an oven overnight and further annealed at 500 ^oC for 3 h under the nitrogen

flow with a heating rate of 1 ^{o}C min^{-1} to obtain carbon coated Fe_3O_4 nanosheets (denoted as Fe_3O_4@C NSs). For comparison, the samples refluxing at 140, 160 and 180 ^{o}C were also prepared to understand the formation mechanism of Fe_3O_4 NSs without changing other conditions.

***Materials characterization*:** The crystal phase of products was characterized by X-ray powder diffraction (XRD) on a Bruker D8 Advanced X-Ray Diffractometer with Ni filtered Cu Kα radiation (λ = 1.5406 Å) at a voltage of 40 kV and a current of 40 mA. Field-emission scanning electron microscope (FESEM) images of the products were acquired on a JEOL JSM-6700F microscope operated at 5 kV. Transmission electron microscope (TEM) images were observed on JEOL JEM-2010 and JEOL JEM-2100F microscopes. Thermogravimetric analysis (TGA) was carried out under air flow of 200 mL min^{-1} with a heating rate of 10 ^{o}C min^{-1}. Nitrogen sorption measurement was performed on Autosorb 6B at liquid N_2 temperature.

Electrochemical measurements: The electrochemical tests were carried out in two-electrode Swagelok cells. The working electrodes consist of 70 wt% of active materials, 20 wt% of conductive carbon black (Super-P-Li), and 10 wt% of polymer binder (polyvinylidene fluoride, PVDF). After magnetic stirring at room temperature for 24 h, the mixing slurry was pasted on copper foil as a current collector, followed by vacuum drying at 120 ^{o}C overnight. The electrolyte is 1 M $LiPF_6$ in a mixture of ethylene carbonate and diethyl carbonate (1:1 by weight). Lithium discs were used as both the counter electrode and reference electrode. Cell assembly was carried out in an Ar-filled glovebox (Innovative Technology Inc.) with moisture and oxygen concentrations below 1.0 ppm. The galvanostatic charge-discharge measurements were performed within a voltage window of 0.01-3 V on a NEWARE battery tester. The cyclic voltammetry measurements were carried out over a potential window of 0.01-3.0 V on an electrochemical workstation (CHI 660D).

3. Results and discussion

The one-spot strategy for synthesizing carbon coated Fe_3O_4 is schematically depicted in **Schematic 1**. During the refluxing, the reaction between ferric chloride ($FeCl_3{\cdot}6H_2O$) and EG happens to form the iron alkoxide ($Fe_2(OCH_2CH_2O)_3$) precursor.[37] Subsequent annealing in nitrogen atmosphere leads to the carbonization of the organic component in the precursor to form amorphous carbon overlayer, and meanwhile the partial reduction of Fe^{3+} to form Fe_3O_4 nanocrystals.[37] As a result, the carbon coated Fe_3O_4 nanocrystals (Fe_3O_4@C) has been formed successfully.

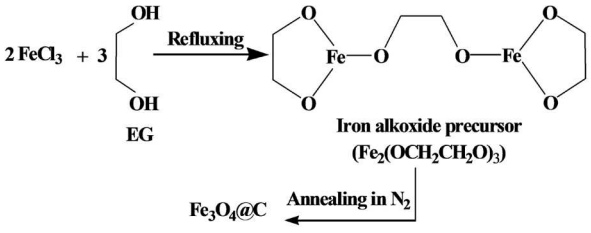

Schematic 1. Schematic illustration of the formation of Fe_3O_4@C product.

The crystallographic structure and phase purity of as-prepared hierarchical Fe_3O_4@C nanosheets are examined by powder X-ray diffraction (XRD) as shown in **Figure 1A**. Obviously, all the identified diffraction peaks in the XRD pattern can be well assigned to the face-centered-cubic magnetic Fe_3O_4 (JCPDS card no. 19-0629).[14, 21, 38] No other additional diffraction peaks from possible impurities are observed, indicating the high phase purity of as-prepared magnetic Fe_3O_4. The morphology and structure of as-prepared Fe_3O_4@C NSs are examined by field-emission scanning electron microscopy (FESEM). **Figure 1B** shows a panoramic view of the Fe_3O_4@C hybrid. Clearly, the hybrid exhibits a large-scale and uniform sheet-like morphology constructed by Fe_3O_4 nanocrystals. In addition, most of the Fe_3O_4 sheets with a size of several microns are flat and isolated each other. The magnified FESEM image (**Figure 1C**) reveals there are some slight crimps at the edge of the flat Fe_3O_4 sheets. **Figure 1D** further demonstrates the thickness of the hybrid sheets is about 60-70 nm via measuring the crimped Fe_3O_4 sheets. Remarkably, some microsized pores can also be observed in the Fe_3O_4 sheets after annealing at 500 ^{o}C as shown in Figure 1D.

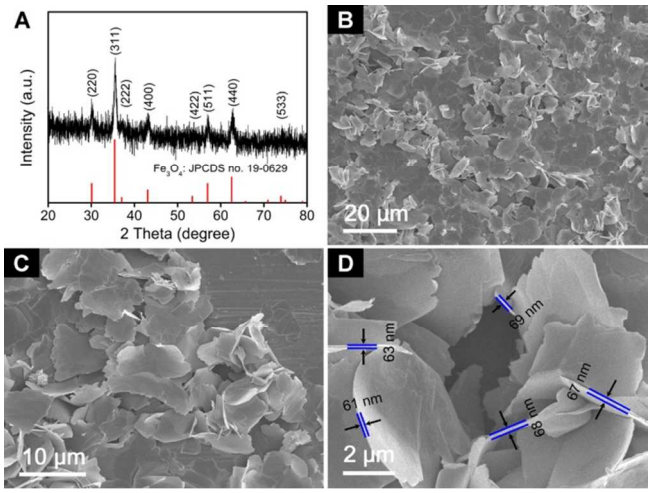

Figure 1. (A) XRD pattern and (B, C, D) FESEM images of carbon coated Fe_3O_4 NSs nanocomposites obtained at 200 ^{o}C.

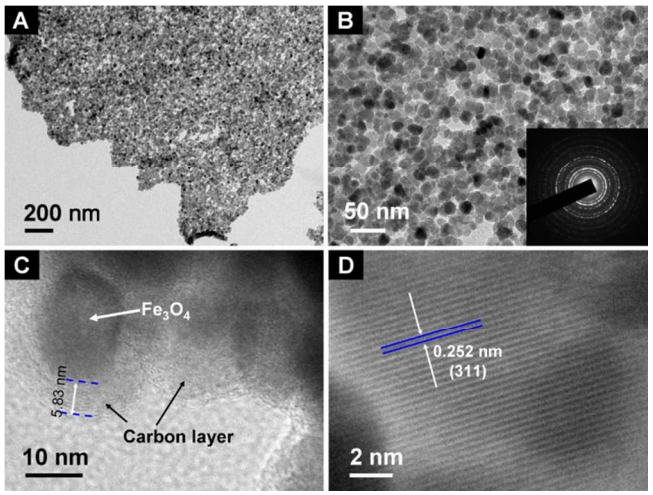

Figure 2. (A, B, C) TEM and (D) HRTEM images (inset of (B) shows SAED pattern) of the carbon coated Fe_3O_4 NSs obtained at 200 ^{o}C.

To provide further insights into the morphology and microstructure of the carbon coated Fe_3O_4 nanosheet composites, transmission electron microcopy (TEM) and high-resolution TEM (HRTEM) images associated with select area electron diffraction (SAED) are shown in **Figure 2**. Consistent with the above FESEM analysis, a low-magnification TEM image (**Figure 2**A) shows an overall view, confirming the large-scale sheet-like morphology of the Fe_3O_4@C hybrid. Interestingly, magnified views of the crystalline Fe_3O_4 nanosheets (**Figure 2**B) clearly reveal the highly porous feature after an annealing treatment at 500 ^{o}C in N_2. Thus a

hierarchical porosity consisting of micropores is produced in the hybrid nanocomposite. The SAED pattern (**inset of Figure 2B**) exhibits a polycrystalline nature and the diffraction rings are readily indexed to the crystal planes of magnetic Fe_3O_4 phase, which is consistent with the XRD result very well. Furthermore, **Figure 2C** clearly demonstrates there is an amorphous carbon overlayer surrounding the Fe_3O_4 nanocrystals, which is derived from the in situ carbonization of the organic components of iron alkoxide precursor ($Fe_2(OCH_2CH_2O)_3$), strongly confirming the in situ formation of carbon nanocoating in this one-pot solution reaction.[16, 24, 25] Moreover, the structural characteristic of a typical Fe_3O_4 nanosheet with visible lattice fringes is distinctly observed in a HRTEM image (**Figure 2D**). The inter-planar distance is measured to be 0.252 nm, corresponding to the (311) crystal planes of the magnetic Fe_3O_4 phase.[22]

The porous feature and pore sizes of as-prepared Fe_3O_4@C NSs nanocomposites were characterized by Brunauer-Emmert-Teller (BET) analysis. As shown in **Figure 3A**, a distinct H4 hysteresis loop can be identified at relative pressures of 0.4-0.95 from the N_2 adsorption-desorption isotherm,[39] suggesting the presence of a mesoporous structure with a high specific surface area of 69.11 $m^2 g^{-1}$. In addition, it can also be observed that the size of the most micropores inside the hierarchical hybrid structure is about 5 nm according to the BJH adsorption branch (**inset of Figure 3A**). Moreover, the carbon content in the hybrid Fe_3O_4@C NSs composites was further determined by thermogravimetric analysis (TGA). As shown in **Figure 3B**, the carbon content is about 10.21 wt% in the hybrid composites after annealing at 500 °C for 3h in N_2. Apparently, both the mesoporous feature with large specific surface area and the amorphous carbon nanocoating are favorable for the electrode materials to deliver excellent electrochemical performance, which will be discussed shortly below.

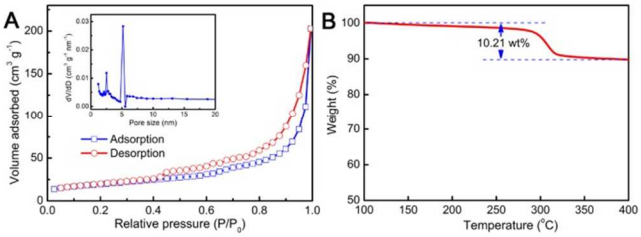

Figure 3. N_2 adsorption-desorption isotherms (A) and thermogravimetric analysis in air (B) of the Fe_3O_4@C NSs, the inset of A shows the pore-size distribution calculated from the BJH adsorption branch.

Interestingly, it is found that the refluxing temperature is crucial for the successful formation of the hierarchical hybrid structure with flat and completely isolated nanosheet subunits of Fe_3O_4. When the refluxing temperature is 140 °C, only uniform sphere-like architecture constructed by dense and interconnecting nanosheet subunits can be observed (**Figure 4A** and **4B**). The diameter of the Fe_3O_4@C hybrid nanospheres is about 2 μm. However, when the temperature increases to 160 °C, the morphology of the Fe_3O_4@C hybrids has evolved into relatively loose flower-like architecture with a large diameter of about 6 μm (**Figure 4C** and **4D**). The entire structure is composed of several dozens of large nanosheets with a thickness of around 70 nm, which are connected with each other through the center to form a 3D flower-like architecture. Upon further increasing the temperature to 180 °C, the flower-like structure of Fe_3O_4@C hybrid is severely destroyed by the high temperature. As a result, most of the interconnected nanosheets become isolated each other as shown in **Figure 4E** and **4F**. Especially under the optimized conduction (200 °C), the flat and completely separate nanosheets in large scale can be successfully obtained as discussed above (Figure 2 and Figure 3). Apparently, the refluxing temperature plays an important role in controlling the formation of the flat and isolated Fe_3O_4@C nanosheets.

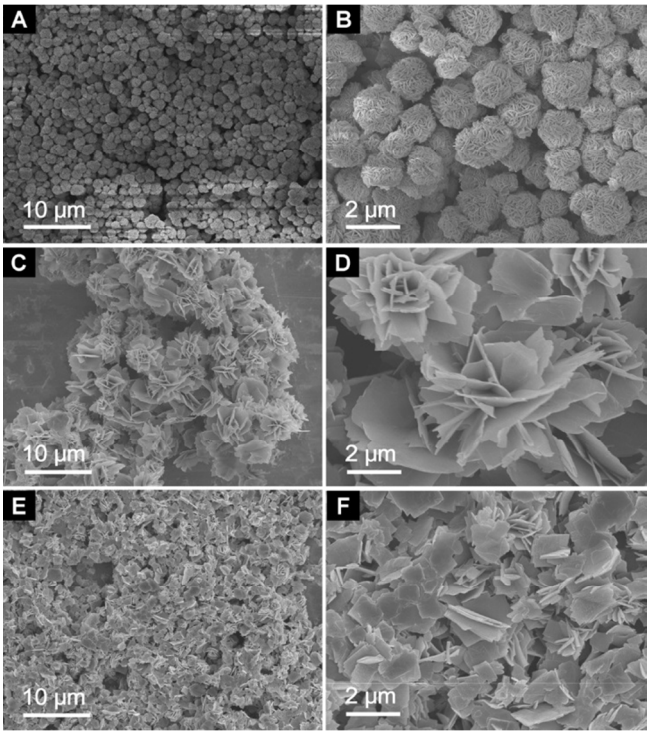

Figure 4. FESEM images of carbon coated Fe_3O_4 hybrids obtained at (A, B) 140 °C, (C, D) 160 °C and (E, F) 180 °C.

We next investigate lithium storage properties of the as-prepared Fe_3O_4@C NSs composites as an anode material for LIBs. **Figure 5A** displays the representative cyclic voltammograms (CVs) for the 1st, 2nd and 5th cycles at a scan rate of 5 mV s^{-1} in the voltage window of 0.01-3.0 V *vs.* Li/Li^+. Consistent with previous literatures, three redox current peaks can be clearly identified from the CVs, suggesting the same lithium storage mechanism according to Fe_3O_4-based anodes.[12, 18, 27, 31] The two distinct reduction peaks located at around 0.55 and 0.81 V in the first cathodic sweep can be ascribed to the reduction of Fe^{3+} or Fe^{2+} to Fe^0 and the formation of amorphous Li_2O plus the irreversible reaction with electrolyte.[39] Obviously, the peak intensity drops significantly in the second cycle, indicating the occurrence of some irreversible electrochemical process in the first cycle. On the other hand, the broad oxidation peak centered at 1.78 V in the anodic sweep, corresponding to the restoration of Fe_3O_4 from Fe^0, exhibits little change in the first five cycles, suggesting good reversibility of the electrochemical reaction.[12, 16, 21, 29, 30]

The typical discharge-charge voltage profiles of Fe_3O_4@C NSs at a constant current density of 200 mA g^{-1} within a cut-off window of 0.01-3.0 V are shown in **Figure 5B**. Remarkably, in agreement with the CV curves, a distinct voltage plateau can be observed at around 0.82 V during the first discharge process.[39] The initial discharge and charge capacities are found to be 1699 and 1069 mAh g^{-1} based on the total sample mass, respectively. The irreversible capacity loss of about 37% may be mainly ascribed to the initial irreversible formation of amorphous Li_2O and other irreversible process such as trapping of some lithium in the lattice, formation of the solid-electrolyte interface (SEI) layer, and electrolyte decomposition, which are common for most anode materials, especially for the nanostructured ones.[38] Nevertheless, from the second cycle onwards, the voltage profiles are approximately overlapping, indicating excellent stability of the hybrid structure for reversible lithium

storage. Besides the high specific capacity, the cycling behavior and rate performance are also very important for LIBs. As shown in **Figure 5C**, the Fe_3O_4@C NSs electrode exhibits excellent cycling stability at the current density of 200 mA g^{-1}. From the second cycle onwards, the discharge capacity of the electrode increases slightly. Even after 120 cycles at 200 mA g^{-1}, a reversible discharge capacity as high as 1232 mAh g^{-1} is still retained, corresponding to 107% of the second-cycle discharge capacity. Such excess discharge capacity can be attributed to the formation of SEI films originated from kinetically activated electrolyte degradation on the one hand.[40-42] Such polymeric gel-like films could provide an extra lithium storage capacity during the charge and discharge process, which is a common phenomenon among many other metal oxides and metal sulfide based anode materials for the LIBs. On the other hand, it is proposed that the lithium storage below the electromotive force value is derived from the interfacial charging mechanism, which could also contribute certain amounts of the extra capacity.[43, 44] To further evaluate the rate capability, the Fe_3O_4@C NSs electrode is cycled at various current densities ranging from 200 to 1000 mA g^{-1} over a voltage window of 0.01-3.0V as shown in **Figure 5D**. The Fe_3O_4@C NSs experience only small decrease in discharge capacity as the current density increases, but still retains high values. For example, the Fe_3O_4@C NSs electrode is still able to deliver a stable discharge capacity of 853 mAh g^{-1} at a high current density of 1000 mA g^{-1}. Remarkably, when the current density is reduced back to 200 mA g^{-1} after more than 50 cycles, a stable high capacity of 1238 mAh g^{-1} can be recovered successfully, indicating outstanding rate capability.

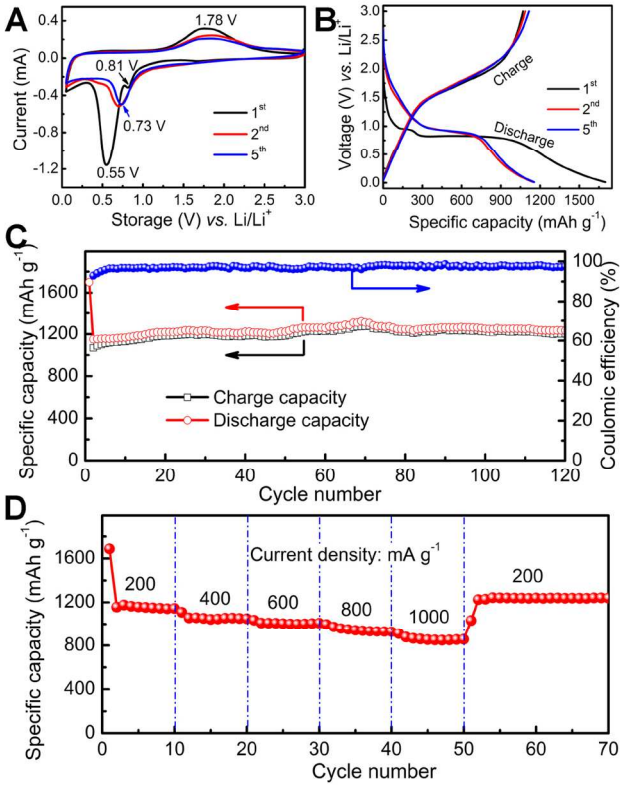

Figure 5. Electrochemical characterization of the optimal carbon coated Fe_3O_4 NSs: (A) CVs at a scan rate of 0.5 mV s^{-1} between 0.01 and 3.0 V, (B) discharge-charge voltage profiles and (C) cycling performance at a current density of 200 mA g^{-1}, and (D) rate capability at different current densities between 0.01 and 3.0 V.

The enhanced cycle stability and rate capability of the Fe_3O_4@C NSs nanocomposite can be attributed to the unique 2D nanostructure and carbonaceous hybrid composition. Specifically, the porous 2D nanosheet structure of Fe_3O_4 is able to provide sufficient electrode-electrolyte contact area for high Li^+ ion flux across the interface and at the same time reduced Li^+ ion diffusion distance, thus greatly facilitating the electrochemical processes especially at high current density.[21] Moreover, the amorphous carbon overlayer surrounding the Fe_3O_4 nanocrystals could improve the structural stability and perhaps the electric conductivity of the electrode materials during the repeated charge-discharge cycling.[20] Benefiting from above advantageous features, the hierarchical hybrid nanostructure of Fe_3O_4@C NSs synthesized in this work could be potentially utilized as a high-performance anode materials in LIBs.

4. Conclusions

We have developed a simple one-pot solution method to synthesize hierarchical Fe_3O_4@C NSs hybrid composites. In this synthesis, the urea severs as alkali source and the ethylene glycol serves as solvent and carbon source. Meanwhile, the refluxing temperature plays an important role to tune the morphology of Fe_3O_4@C hybrid. Especially refluxing at 200 ^oC for 1 h, the flat and separate Fe_3O_4@C nanosheet could be obtained in large scale. When evaluated as an anode material for lithium-ion batteries (LIBs), the hybrid Fe_3O_4@C NSs demonstrate high reversible capacities of 1232 mAh g^{-1} over 120 cycles at the current density of 200 mA g^{-1}, and remarkable rate capability. The present results again suggest that the structural design of electrodes will have important implications on the synthesis of high-performance electrode materials for LIBs.

Acknowledgement

This research was supported partially by the National Natural Science Foundation of China (No. 51273158, 21303131); Natural Science Basis Research Plan in Shaanxi Province of China (No. 2012JQ6003, 2013KJXX-49); Ph.D. Programs Foundation of Ministry of Education of China (No. 20120201120048); Program for New Century Excellent Talents in University (NCET-13-0449). The authors are grateful to the Fundamental Research Funds for the Central Universities for financial support.

Notes and references

Department of Applied Chemistry, School of Science, State Key Laboratory for Mechanical Behavior of Materials, Xi'an Jiaotong University, Xi'an 710049, P. R. China.
E-mail: guoxingao@mail.xjtu.edu.cn (G. X. Gao);
dingsj@mail.xjtu.edu.cn (S. J. Ding)

1. X. W. Lou, L. A. Archer and Z. C. Yang, *Adv. Mater.*, 2008, **20**, 3987.
2. S. Q. Wang, Z. D. Lu, D. Wang, C. G. Li, C. H. Chen and Y. D. Yin, *J. Mater. Chem.*, 2011, **21**, 6365.
3. J. B. Goodenough and K. S. Park, *J. Am. Chem. Soc.*, 2013, **135**, 1167.
4. H. B. Wu, J. S. Chen, H. H. Hng and X. W. Lou, *Nanoscale*, 2012, **4**, 2526.
5. J. Jiang, Y. Y. Li, J. P. Liu, X. T. Huang, C. Z. Yuan and X. W. Lou, *Adv. Mater.*, 2012, **24**, 5166.
6. Y. J. Fu, X. W. Li, X. L. Sun, X. H. Wang, D. Q. Liu and D. Y. He, *J. Mater. Chem.*, 2012, **22**, 17429.
7. W. S. Wang, Q. N. Sa, J. H. Chen, Y. Wang, H. J. Jung and Y. D. Yin, *ACS Appl. Mater. Interfaces*, 2013, **5**, 6478.
8. J. P. Liu, Y. Y. Li, H. J. Fan, Z. H. Zhu, J. Jiang, R. M. Ding, Y. Y. Hu and X. T. Huang, *Chem. Mater.*, 2010, **22**, 212.
9. G. X. Gao, L. Yu, H. B. Wu and X. W. Lou, *Small*, 2014, **10**, 1741.
10. K. J. Zhang, P. X. Han, L. Gu, L. X. Zhang, Z. H. Liu, Q. S. Kong, C. J. Zhang, S. M. Dong, Z. Y. Zhang, J. H. Yao, H. X. Xu, G. L. Cui and L. Q. Chen, *ACS Appl. Mater. Interfaces*, 2012, **4**, 658.
11. L. Wang, Y. H. Li, Z. D. Han, L. Chen, B. Qian, X. F. Jiang, J. Pinto and G. Yang, *J. Mater. Chem. A*, 2013, **1**, 8385.
12. B. Lim, J. Jin, J. Yoo, S. Y. Han, K. Kim, S. Kang, N. Park, S. M. Lee, H. J. Kim and S. U. Son, *Chem. Commun.*, 2014, **50**, 7723.

13. J. Tucek, K. C. Kemp, K. S. Kim and R. Zboril, *ACS Nano*, 2014, **8**, 7571.
14. Y. R. Wang, L. Zhang, X. H. Gao, L. Y. Mao, Y. Hu and X. W. Lou, *Small*, 2014, **10**, 2815.
15. L. Wang, L. Zhuo, C. Zhang and F. Zhao, *Chem. Eur. J.*, 2014, **20**, 4308.
16. H. G. Deng, S. L. Jin, L. Zhan, M. L. Jin and L. C. Ling, *New Carbon Mater.*, 2014, **29**, 301.
17. K. Cheng, F. Yang, K. Ye, Y. Zhang, X. Jiang, J. L. Yin, G. L. Wang and D. X. Cao, *J. Power Sources*, 2014, **258**, 260.
18. A. P. Hu, X. H. Chen, Q. L. Tang and B. Zeng, *Ceram. Int.*, 2014, **40**, 14713.
19. Y. G. Zhu, J. Xie, G. S. Cao, T. J. Zhu and X. B. Zhao, *RSC Adv.*, 2013, **3**, 6787.
20. K. Y. Xie, Z. G. Lu, H. T. Huang, W. Lu, Y. Q. Lai, J. Li, L. M. Zhou and Y. X. Liu, *J. Mater. Chem.*, 2012, **22**, 5560.
21. H. B. Geng, Q. Zhou, J. W. Zheng and H. W. Gu, *RSC Adv.*, 2014, **4**, 6430.
22. L. L. Wang, J. W. Liang, Y. C. Zhu, T. Mei, X. Zhang, Q. Yang and Y. T. Qian, *Nanoscale*, 2013, **5**, 3627.
23. Y. M. Sun, X. L. Hu, W. Luo and Y. H. Huang, *J. Mater. Chem.*, 2012, **22**, 19190.
24. Q. Gao, A. W. Zhao, Z. B. Gan, W. Y. Tao, D. Li, M. F. Zhang, H. Y. Guo, D. P. Wang, H. H. Sun, R. R. Mao and E. H. Liu, *Crystengcomm*, 2012, **14**, 4834.
25. L. H. Han, Y. C. Chen and Y. Wei, *Crystengcomm*, 2012, **14**, 4692.
26. D. Q. Liu, X. Wang, X. B. Wang, W. Tian, J. W. Liu, C. Y. Zhi, D. Y. He, Y. Bando and D. Golberg, *J. Mater. Chem. A*, 2013, **1**, 1952.
27. C. X. Wang, G. J. Shao, Z. P. Ma, S. Liu, W. Song and J. J. Song, *Electrochim. Acta*, 2014, **130**, 679.
28. J. P. Zhao, B. J. Yang, Z. M. Zheng, J. Yang, Z. Yang, P. Zhang, W. C. Ren and X. B. Yan, *ACS Appl. Mater. Interfaces*, 2014, **6**, 9890.
29. M. M. Liu and J. Sun, *J. Mater. Chem. A*, 2014, **2**, 12068.
30. S. M. Abbas, S. Ali, N. A. Niaz, N. Ali, R. Ahmed and N. Ahmad, *J. Alloys Compd.*, 2014, **611**, 260.
31. Y. P. Gan, H. Q. Gu, H. Xiao, Y. Xia, X. Y. Tao, H. Huang, J. Du, L. S. Xu and W. K. Zhang, *New J. Chem.*, 2014, **38**, 2428.
32. S. M. Yuan, J. X. Li, L. T. Yang, L. W. Su, L. Liu and Z. Zhou, *ACS Appl. Mater. Interfaces*, 2011, **3**, 705.
33. L. M. Lang and Z. Xu, *ACS Appl. Mater. Interfaces*, 2013, **5**, 1698.
34. D. Y. Park and S. T. Myung, *ACS Appl. Mater. Interfaces*, 2014, **6**, 11749.
35. P. P. Lv, H. L. Zhao, Z. P. Zeng, J. Wang, T. H. Zhang and X. W. Li, *J. Power Sources*, 2014, **259**, 92.
36. Y. C. Ma, Y. D. Huang, X. C. Wang, D. Z. Jia and X. C. Tang, *J. Nanopart. Res.*, 2014, **16**.
37. L. S. Zhong, J. S. Hu, H. P. Liang, A. M. Cao, W. G. Song and L. J. Wan, *Adv. Mater.*, 2006, **18**, 2426.
38. X. Y. Li, X. L. Huang, D. P. Liu, X. Wang, S. Y. Song, L. Zhou and H. J. Zhang, *J. Phys. Chem. C*, 2011, **115**, 21567.
39. Q. Zhou, Z. B. Zhao, Z. Y. Wang, Y. F. Dong, X. Z. Wang, Y. Gogotsi and J. S. Qiu, *Nanoscale*, 2014, **6**, 2286.
40. X. W. Li, S. L. Xiong, J. F. Li, X. Liang, J. Z. Wang, J. Bai and Y. T. Qian, *Chem-Eur J*, 2013, **19**, 11310.
41. Y. M. Sun, X. L. Hu, W. Luo, F. F. Xia and Y. H. Huang, *Adv Funct Mater*, 2013, **23**, 2436.
42. W. M. Zhang, X. L. Wu, J. S. Hu, Y. G. Guo and L. J. Wan, *Adv Funct Mater*, 2008, **18**, 3941.
43. K. F. Zhong, B. Zhang, S. H. Luo, W. Wen, H. Li, X. J. Huang and L. Q. Chen, *J. Power Sources*, 2011, **196**, 6802.
44. X. Q. Yu, Y. He, J. P. Sun, K. Tang, H. Li, L. Q. Chen and X. J. Huang, *Electrochem Commun*, 2009, **11**, 791.

Graphical Abstract

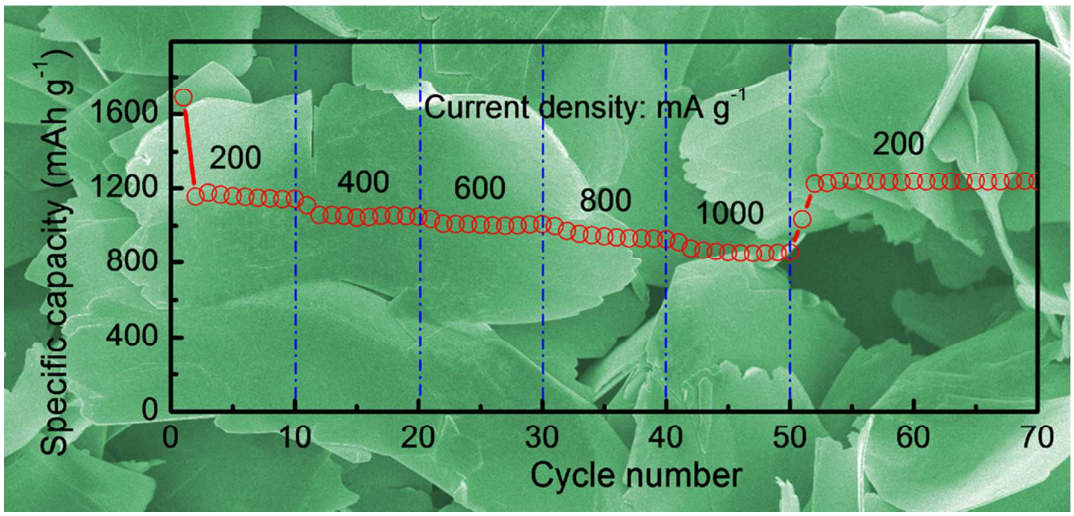

A large-scale flat Fe_3O_4 nanosheets coated by amorphous carbon overlayer (denoted as Fe_3O_4@C NSs) was prepared via a simple one-pot solution method followed by a thermal annealing treatment using ethylene glycol as the solvent and carbon source. When evaluated as an anode material for LIBs, the as-prepared Fe_3O_4@C NSs hybrid composites exhibit remarkable lithium storage properties with high specific capacity, good cycling stability and excellent rate capability.